Dependence of domain wall stability on vortex chirality in asymmetric nanoring

X. H. Wang, S. Goolaup, and W. S. Lew[a)]
School of Physical and Mathematical Sciences, Nanyang Technological University, 21 Nanyang Link, Singapore 637371

(Received 19 July 2010; accepted 17 September 2010; published online 5 October 2010)

We report on the direct observation of notch-free domain wall (DW) trapping and field history effect on the DW behavior in $Ni_{80}Fe_{20}$ asymmetric ring. We found that a 360° DW is trapped at the narrow arm while the ring adopts a vortex configuration. The stability of DW is dependent on the chirality of the vortex state and the external field direction. A 360° DW trapped in a clockwise vortex configuration is highly resistant to annihilation upon the application of $+x$ field; the 360° DW trapped in an anticlockwise vortex breaks apart with a small $+x$ field. © *2010 American Institute of Physics*. [doi:10.1063/1.3498026]

Magnetic nanostructures[1] created by controlled nanofabrication techniques are attracting intense research interest due to their potential significance in magnetic data storage,[2] and solid state memory[3] devices. Toward achievable applications of these devices, a stable and reproducible switching mechanism is needed for the nanomagnets. Of all the studied nanostructures, ring-shaped nanomagnets have reproducible magnetic states, that arise from a competition[4] between the magnetostatic energy and the exchange energy. The ring structure also prohibits the formation of edge domains and minimizes the stray field. This makes the ring structure an ideal candidate for use in ultra high density data storage. The switching process in ring structures is by the formation of the "onion" state,[6] followed by the vortex state[5] occurring via the movement of domain wall (DW). One difficulty associated with the ring structures during the reversal process is the inability to pin the DW that is nucleated in a certain position in the symmetric rings. An approach that is commonly used to pin the DWs is by exploiting the shape anisotropy, e.g., the use of elliptically shaped ring structures.[7] Alternatively, the DW can be pinned via the creation of geometrical defects or notches[8] along the ring structure. Such notches introduce low energy well to interrupt the continuity of the magnetization.

Asymmetric ring (ASR) is also an interesting candidate for DW pinning, as it possess not only all the intriguing spin configurations of a symmetric ring but its asymmetry induces new properties. We have previously theoretically predicted that the chirality of a vortex state in an asymmetric nanoring can be controlled, by exploiting the asymmetric feature. Below a critical film thickness, a DW can be trapped at the narrow arm of the ASR structure.[9]

In this letter, we report on the direct observation of the motion of a 360° DW in ASRs. To study the reversal mechanism experimentally, a 10-nm-thick $Ni_{80}Fe_{20}$ ASR-shaped nanomagnets array was fabricated using electron beam lithography technique. Magnetron sputtering technique was used to deposit Ta (5 nm)/$Ni_{80}Fe_{20}$ (10 nm)/Ta (5 nm) films. To minimize the degradation of the $Ni_{80}Fe_{20}$ (NiFe) layer, Ta film was used as both a buffer and capping layer. The NiFe film thickness of 10 nm was selected based on our previous simulation result.[9] During deposition, the chamber base pressure was better than 3.0×10^{-8} Torr, and the sputtering pressure was maintained at 3 mTorr. Shown in Fig. 1 is the scanning electron micrograph (SEM) image of the 10 nm thick NiFe ASR shaped nanomagnet array. The outer diameter of the fabricated ASR structure is 1200 nm while the inner diameter is 600 nm. The asymmetry is induced by offsetting the center of the inner circle by a distance ($l=120$ nm) with respect to the center of the outer circle, as shown schematically in the inset of Fig. 1. The rings were patterned with a spacing of 2400 nm to eliminate any magnetostatic field coupling among the nanomagnets.

Shown in Fig. 2 is a normalized hysteresis loop of the 10-nm-thick NiFe asymmetric nanorings measured by magneto-optical Kerr effect (MOKE) magnetometry. The field was applied along the x-axis, as depicted in the inset of Fig. 1. Also shown in Fig. 2 is the simulated hysteresis loops and the corresponding spin configurations, which were obtained from OOMMF[10] simulations. The intrinsic parameters for NiFe were used in the simulation; crystalline anisotropy constant $K_1=0$, saturation magnetization $M_s=8.6 \times 10^5$ A m^{-1}, exchange stiffness $A=1.3\times 10^{-11}$ J m^{-1},

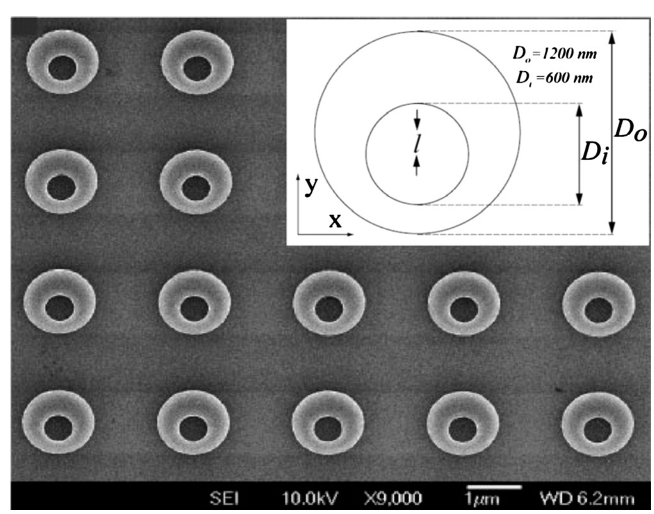

FIG. 1. SEM of a 10-nm-thick $Ni_{80}Fe_{20}$ ASR array. The outer diameter D_o of the ASR is 1200 nm, the inner diameter D_i is 600 nm and the offset from the center is 120 nm. Inset shows the geometric model.

[a)]Electronic mail: wensiang@ntu.edu.sg.

 © 2010 American Institute of Physics

Downloaded 02 Dec 2010 to 155.69.4.4. Redistribution subject to AIP license or copyright; see http://apl.aip.org/about/rights_and_permissions

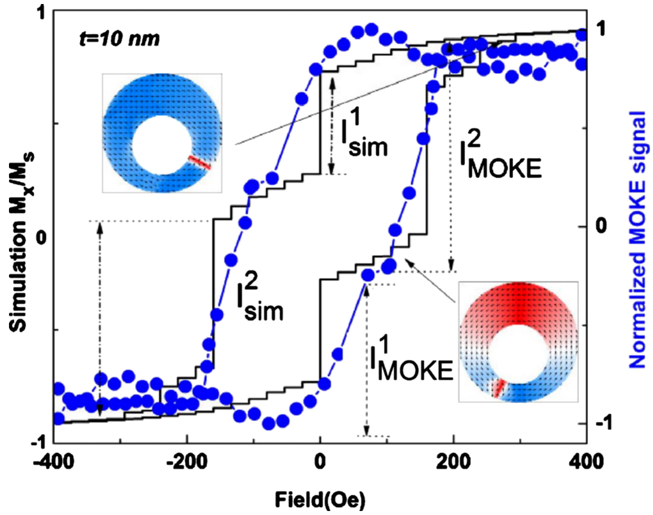

FIG. 2. (Color online) Normalized MOKE hysteresis loop for a 10-nm-thick $Ni_{80}Fe_{20}$ ASRs superimposed with simulated hysteresis loops. Insets show the corresponding simulated spin configurations.

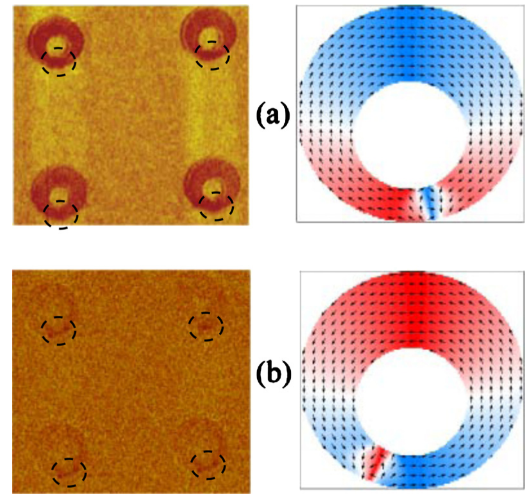

FIG. 3. (Color online) MFM images and simulated configurations of (a) clockwise and (b) anticlockwise vortex states with the 360° DW at the narrow of the 10-nm-thick $Ni_{80}Fe_{20}$ ASR, when the external field is 0 Oe.

damping coefficient $\alpha=0.5$. The cell size was set to 5 nm.

The simulated hysteresis loop is characterized by two major steps of different magnitudes. The plateau which results from an increase in magnetization at 0 Oe, is due to the formation of a DW trapping vortex configuration. The spins are oriented circularly around the circumference of the ring, with a 360° DW at the narrow arm, as seen from the simulated spin state. The plateau extends until a field of around +200 Oe. The 360° DW trapped at the narrow arm does not annihilate until a large reversal field of +300 Oe is applied. The small step at larger field region is due to the annihilation of the trapped DW at the narrow arm. The MOKE hysteresis measurement of the ASR reveals a gradual switch in magnetization in the field range of +50 Oe to +130 Oe. This switch is associated with the formation of the 360° DW trapping vortex state in the ring structure, similar to the plateau region seen in the simulation. The magnitude of the MOKE signal intensity from the first switch I^1_{MOKE} is smaller than that of the second switch, $I^1_{\mathrm{MOKE}}/I^2_{\mathrm{MOKE}}=0.55$ which is close to the ratio, obtained from the simulation; $I^1_{\mathrm{Sim}}/I^2_{\mathrm{Sim}}=0.6$.

The magnitude difference of the switch reflects the selective transverse DW movement, when the ring evolves from the onion to the DW trapping state. Since the DW energy[11] is dependent on the ring arm width, the transverse wall in the onion state, will always move to the narrow arm of the ASR. This DW selective movement can be used to control the chirality of the vortex state in the ASR. The chirality of the vortex configuration is determined by the initial direction of the magnetization along the wider arm of the ASR during saturation; when the wider arm has spins along the $+x$ $(-x)$ direction, the resulting chirality of the vortex will be clockwise (anticlockwise). It is worth pointing out that due to the small magnetic moment of the trapped DW, our MOKE measurement was not able to resolve the presence of the small step at high field prior to its annihilation.

To directly observe the magnetic states and the chirality control features in the ASR structure during the reversal process, we have carried out magnetic force microscopy (MFM) imaging. A lift scan height of 50 nm was used for all the measurements. Shown in Fig. 3 are the representative MFM images and the corresponding simulated states at remanence for the ASR. By applying a large saturation field along the $+x$ (or $-x$) direction and reducing to 0 Oe, two states with bright and dark contrast vortex were observed. The dark and bright contrast corresponds to clockwise and anticlockwise chirality of the vortex, respectively. In both cases a DW is trapped at the narrow arm. The MFM measurement confirms the DW trapping feature in the ASR predicted by our simulation.

To study how the vortex chirality affects the stability of the 360° DW in the ASR, the magnetic states were imaged as a function of a sweeping *in situ* magnetic field. Starting from the bright/dark contrast vortex state, the *in situ* magnetic field was increased along the $+x$ direction. For the clockwise vortex state, the DW at the narrow arm remains trapped as the external field is increased up to +100 Oe. Figure 4(a) shows the MFM image of the ASR array when the *in situ* field is +100 Oe. The dark contrast at the narrow arm corresponds to the trapped DW. As the *in situ* magnetic field is increased to +200 Oe, we observed the formation of a second DW at the wider arm, as seen in Fig. 4(b). Increasing the field to +300 Oe, leads to the annihilation of the DW at the wider arm while the trapped DW at the narrow arm can still be observed, as seen as the dark contrast at the narrow arm in Fig. 4(c). Simulation reveals that when the chirality is clock-

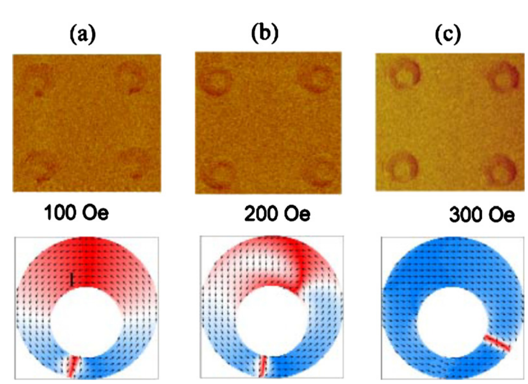

FIG. 4. (Color online) MFM images of the field driven DW motion in the clockwise DW trapping vortex configuration, as the *in situ* magnetic field is applied in the $+x$ axis. The corresponding simulated spin configurations are shown in the lower panel.

Downloaded 02 Dec 2010 to 155.69.4.4. Redistribution subject to AIP license or copyright; see http://apl.aip.org/about/rights_and_permissions

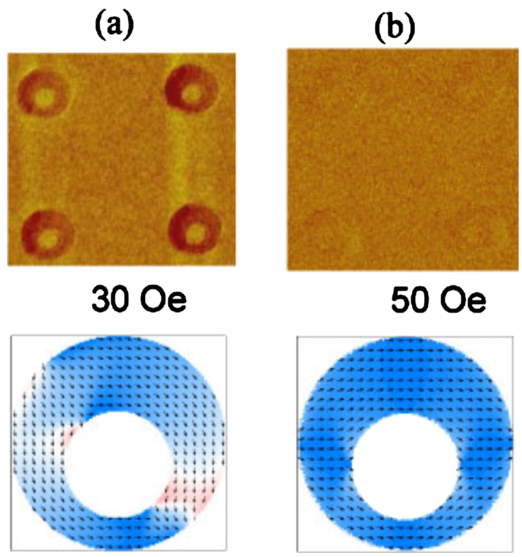

FIG. 5. (Color online) MFM images of the 360° DW motion, trapped within a vortex configuration with anticlockwise chirality in the 10 nm $Ni_{80}Fe_{20}$ ASR as a function of *in situ* magnetic field applied in the $-x$ axis. The lower panel shows the corresponding simulated spin configurations.

wise, applying a magnetic field in the $+x$ direction does not annihilate the trapped DW. Instead, an additional DW is nucleated at the wide part of the ring. As the reversal field is further increased to +300 Oe, the DW at the wide arm annihilates leaving the persistently trapped DW at the narrow arm. The simulation results are in good agreement with our MFM observation.

For the DW trapped in anticlockwise vortex, the external magnetic field influences the trapped DW more significantly. Applying a small reversal field of +30 Oe disrupts the trapped DW and an "onion" state is formed. The dark contrast in the MFM image in Fig. 5(a), measured with an *in situ* field of +30 Oe, corresponds to the two DWs in the "onion" state. When a reversal field of +50 Oe is applied, the ASR array exhibits a low contrast. The micromagnetic simulation shows that when the vortex state is anticlockwise, a field of +30 Oe breaks the trapped 360° DW into two transverse walls. The separated DWs move apart and forming a tilted "onion" state. When the reversal field increases to +50 Oe, the ASR array adopts a negative saturation as shown in Fig. 5(b). From the MFM scanning and the simulation, the stability of the DW trapped in the vortex state is strongly dependent on the chirality of the vortex.

In summary, we have performed detailed studies on the DW trapping behavior and the field effect on the trapped DW in an asymmetric magnetic ring. By analyzing our experimental observations with the aid of micromagnetic simulation, we have been able to identify that a 360° DW is trapped at the narrow arm when the ring adopts the vortex configuration. We found that the DW stability is strongly dependent on the vortex chirality of the ASR. This nongeometric defect DW trapping behavior in the ASR structure can be useful in the applications of DW devices.

This work was supported in part by the ASTAR SERC Grant (Grant No. 082 101 0015) and the NRF-CRP program (Multifunctional Spintronic Materials and Devices). Electron beam lithography was supported by the NanoFabrication and Characterization Facility (SNFC) at the Institute of Materials Research and Engineering (IMRE, ASTAR). The authors thank Dr. Deng Jie and Miss Teo Siew Lang for their assistance in the nanopatterning process.

[1]R. P. Cowburn, J. Phys. D: Appl. Phys. **33**, R1 (2000).
[2]A. Wachowiak, J. Wiebe, M. Bode, O. Pietzsch, M. Morgenstern, and R. Wiesendanger, Science **298**, 577 (2002).
[3]S. Tehrani, B. Engel, J. M. Slaughter, E. Chen, M. DeHerrera, M. Durlam, P. Naji, R. Whig, J. Janesky, and J. Calder, IEEE Trans. Magn. **36**, 2752 (2000).
[4]M. Klaui, C. A. F. Vaz, L. Lopez-Diaz, and J. A. C. Bland, J. Phys.: Condens. Matter **15**, R985 (2003).
[5]J. Rothman M. Klaui L. Lopez-Diaz, C. A. Vaz, A. Bleloch, J. A. C. Bland, Z. Cui, and R. Speaks, Phys. Rev. Lett. **86**, 1098 (2001).
[6]S. P. Li, D. Peyrade, M. Natali, A. Lebib, Y. Chen, U. Ebels, L. D. Buda, and K. Ounadjela, Phys. Rev. Lett. **86**, 1102 (2001).
[7]F. J. Castaño, C. A. Ross, and A. Eilez, J. Phys. D: Appl. Phys. **36**, 2031 (2003).
[8]M. Klaui, C. A. F. Vaz, J. A. C. Bland, W. Wernsdorfer, G. Faini, E. Cambril, L. J. Heyderman, F. Nolting, and U. Rüdiger, Phys. Rev. Lett. **94**, 106601 (2005).
[9]X. H. Wang, W. K. Peng, and W. S. Lew, J. Appl. Phys. **106**, 043905 (2009).
[10]The software is available at http://math.nist.gov/oommf.
[11]F. Q. Zhu, G. W. Chern, O. Tchernyshyov, X. C. Zhu, and C. L. Chien, Phys. Rev. Lett. **96**, 027205 (2006).

Downloaded 02 Dec 2010 to 155.69.4.4. Redistribution subject to AIP license or copyright; see http://apl.aip.org/about/rights_and_permissions